PCCP

Accepted Manuscript

ROYAL SOCIETY OF CHEMISTRY

www.rsc.org/pccp

Table of contents entry

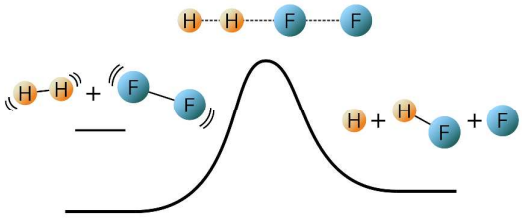

The reactivity is significantly enhanced by vibrational excitation of F_2 whereas excitation of H_2 vibration has a moderate effect.

Mode Selective Dynamics and Kinetics of the $H_2 + F_2 \rightarrow H + HF + F$ Reaction

Akira Matsugi*[a] and Toshiyuki Takayanagi[b]

[a] *National Institute of Advanced Industrial Science and Technology (AIST), 16-1 Onogawa, Tsukuba, Ibaraki 305-8569, Japan. E-mail: a.matsugi@aist.go.jp*

[b] *Department of Chemistry, Saitama University, 255 Shimo-Okubo, Sakura-ku, Saitama City, Saitama 338-8570, Japan*

Electronic Supplementary Information (ESI) available: Figure S1 describing equipotential contour plots of the $H_2 + F_2$ reaction on the trapezoidal configuration and Figure S2 showing collinear reaction probabilities for the $H_2 + F_2 \rightarrow H + HF + F$ reaction as a function of the translational energy. See DOI: [doi].

Abstract

The reaction between vibrationally excited H_2 and F_2 had previously been suggested to be a critical chain-branching step in the combustion of mixtures containing H_2 and F_2. In the present study, the vibrational state specific dynamics and kinetics for the reaction $H_2 + F_2 \rightarrow H + HF + F$ (R1) were investigated by quasiclassical trajectory (QCT) and quantum mechanical (QM) reactive scattering calculations on an accurate potential energy surface that was constructed based on a large number of quantum chemical calculations at the MRCI-F12(CV)+Q / cc-pCVTZ-F12 level. The reaction probabilities for R1 in collinear configurations were obtained from the QCT and QM calculations, and the state specific rate constants were evaluated by the full-dimensional QCT calculations. Both the collinear and full-dimensional results demonstrated that R1 can be significantly promoted by vibrational excitation of F_2, whereas excitation of H_2 vibration has a smaller effect on the reactivity. This indicates that the rate constants for the presumed chain-branching reaction, H_2 ($\nu = 1$) + $F_2 \rightarrow H + HF + F$, used in the previous kinetic modeling study of H_2/F_2 combustion was overestimated. The mode-selective reactivity observed for R1 was interpreted in terms of the coupling between the vibrational modes of the reactants and the reaction coordinate motion.

1. Introduction

The reaction between hydrogen and fluorine molecules,

$$H_2 + F_2 \rightarrow H + HF + F \qquad (R1)$$

has been suggested to play a critical role, as a chain-branching reaction, in the combustion of H_2/F_2 mixtures.[1,2] The proposed chain-reaction mechanism can be summarized as:

$$H + F_2 \rightarrow HF(\nu = 0–8) + F \qquad (R2)$$

$$F + H_2 \rightarrow HF(\nu = 1–3) + H \qquad (R3)$$

$$HF(\nu) + M \rightarrow HF\,(\nu–1) + M \qquad (R4)$$

$$HF(\nu = 1) + H_2 \rightarrow HF + H_2(\nu = 1) \qquad (R5)$$

$$H_2(\nu = 1) + F_2 \rightarrow H + HF + F \qquad (R1')$$

where, ν denotes the diatomic vibrational quantum number. The reactions $H + F_2$ and $F + H_2$ are known to generate vibrationally excited HF, resulting in a significant amount of $HF(\nu > 0)$ being present during H_2/F_2 combustion. Vibrationally excited H_2 can also be produced as a result of the V–V energy-transfer reaction between $HF(\nu = 1)$ and H_2, R5. Owing to there being just a small energy change in R5, the deactivation of $HF(\nu = 1)$ by H_2 is expected to predominantly occur through the V–V exchange process.[3,4] Consequently, the reaction between H_2 ($\nu = 1$) and F_2, directly producing H + HF + F, was suggested to be an important chain-branching step.

The kinetic modeling study by Sullivan et al.,[2] who simulated the second explosion limits in H_2/F_2 mixtures,[5] suggested a rate constant of (1–3) × 10^{-19} cm^3 s^{-1} for R1' at 350 K. The rate constant was also estimated by a thermometric technique to be (7.5 ± 1.5) × 10^{-20} cm^3 s^{-1} at 310 K.[6] In a recent kinetic modeling study of the burning velocities for $H_2/F_2/O_2/N_2$ flames,[1] R1' had to be included in the model to reproduce the experimental burning velocities. By comparing simulated burning velocities to experimentally obtained ones, the activation energy of R1 was

estimated to be 59 kJ mol^{-1},[1] which was evaluated assuming the rate constant at 310 K to be 7.5 $\times 10^{-20}$ cm^3 s^{-1}.[6]

There have been only two computational studies reported for R1. A quasiclassical trajectory (QCT) study by Thompson and McLaughlin[7] using a semiempirical potential energy surface (PES) revealed qualitative features of the reaction. Their PES indicated two reaction paths, a collinear channel leading to H + HF + F products and a trapezoidal channel leading to 2HF. The QCT calculations suggested that the rate constants for both channels significantly increase with an increase in the initial vibrational energy of H_2, and that the 2HF channel is kinetically dominant over the H + HF + F channel. However, the transition state for the trapezoidal channel could not be located by the recent quantum chemical calculation carried out at the multireference configuration interaction (MRCI) level.[1] The MRCI calculation identified only a collinear H-H-F-F transition state for R1 with a barrier height of 113 kJ mol^{-1}. This barrier height was 54 kJ mol^{-1} larger than the activation energy for R1' estimated by the kinetic modeling of the burning velocities,[1] and this difference is comparable to the energy gap between $H_2(v = 1)$ and $H_2(v = 0)$ (4161 cm^{-1} = 50 kJ mol^{-1}). However, since the effect of vibrational excitations on reactivity depend largely on the topological features of the PES, a detailed dynamics study is needed to elucidate the kinetics of R1'.

In the present study, the dynamics and kinetics of the $H_2 + F_2$ reaction were investigated on a global PES constructed by extensive quantum chemical calculations at the MRCI level. The rate constants for R1 were evaluated by full-dimensional QCT calculations and transition state theory (TST) on the PES. The QCT calculations enabled examination of the effects of the vibrational excitations of H_2 and F_2 on the rate constants. The reaction probabilities were also calculated by quantum mechanical (QM) reactive scattering calculation with restricted collinear

configuration, and compared with the QCT results.

2. Methods

2.1. Quantum Chemical Calculation

Quantum chemical calculations of R1 were performed using an explicitly correlated internally contracted multireference configuration interaction (MRCI-F12) method[8–10] with Davidson's quadruples correction (Q). The reference molecular orbitals were obtained from a full-valence (16 electrons are distributed in 10 active orbitals) complete active space self-consistent field (CASSCF) calculation. At some regions on the PES, the orbitals which correlate with the 2*s* orbitals of the F atoms were found to mix with the closed-shell orbitals arising from the 1*s* orbitals of the F atoms. This effect resulted in an artificially large correlation energy when the core orbitals were not correlated[11,12]; therefore, though the core orbitals were constrained to be doubly occupied in CASSCF, the core-valence correlation (CV) was included in the MRCI calculation.

The explicitly correlated F12 method[10,13,14] was adopted because it has been shown to yield results with near-complete basis set limit accuracy with triple-ζ basis sets, whereas conventional methods require at least quintuple-ζ basis sets. This dramatically improved convergence is achieved by introducing terms into the wave function that explicitly depend on the inter-electron distances. A correlation-consistent triple-ζ basis set optimized for describing core-valence correlation effects with explicitly correlated methods, cc-pCVTZ-F12,[15] was used throughout the present study. The cc-pCVTZ-F12/OptRI[15] was used as a complementary auxiliary basis set. The cc-pVTZ/JKFIT[16] and aug-cc-pwCVTZ/MP2FIT[17,18] auxiliary basis sets were employed for

the density fitting.

All quantum chemical calculations were carried out using the Molpro program.[19] The method described here, which can be referred to as MRCI-F12(CV)+Q / cc-pCVTZ-F12, is hereafter abbreviated as MRCI in this paper.

As previously reported,[1] MRCI identified a collinear H-H-F-F transition state that is directly correlated to the H_2 + F_2 reactants and the H + HF + F products. The HH, HF, and FF bond lengths of the transition state were 0.865, 1.159, and 1.729 Å, respectively. Figure 1 shows an energy diagram for R1. The vibrational energy levels of the reactants and product calculated from the molecular constants[20] are also shown. Here, v_{HH}, v_{FF}, and v_{HF} represent the vibrational quantum numbers for H_2, F_2, and HF, respectively. The reaction is endothermic by 18 kJ mol^{-1}. The barrier height was computed to be 112 and 103 kJ mol^{-1} for the potential and vibrational ground state energies, respectively.

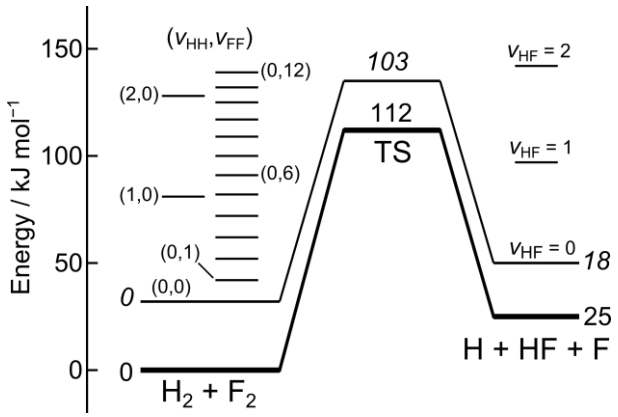

Figure 1. Energy diagram for the H_2 + F_2 → H + HF + F reaction. The thick and thin lines represent the MRCI potential and vibrational ground state energetics. The energies are shown relative to the potential energy of the reactant asymptote except those shown in *italic*, which

represent the relative vibrational ground state energies. The vibrational energy levels of reactants and product are also drawn.

2.2. Construction of Potential Energy Surface

The PES was constructed using a polynomial expansion method developed by Bowman and co-workers.[21–23] The six-dimensional PES was represented in the form of an eighth-order, direct products, multinomial in Morse variable for six internuclear distances,

$$V(y_1, y_2, \cdots, y_6) = \sum_{N_{\text{order}} \leq 8} C_{n_1 n_2, \cdots, n_6} y_1^{n_1} y_6^{n_6} \left(y_2^{n_2} y_3^{n_3} y_4^{n_4} y_5^{n_5} + y_3^{n_2} y_2^{n_3} y_5^{n_4} y_4^{n_5} + y_4^{n_2} y_5^{n_3} y_2^{n_4} y_3^{n_5} + y_5^{n_2} y_4^{n_3} y_3^{n_4} y_2^{n_5} \right) \quad (1)$$

where $y_i = \exp(-r_i / 2.0 \text{ bohr})$ for $i = 1$–6, r_i are the internuclear distances, and $N_{\text{order}} = n_1 + n_2 + n_3 + n_4 + n_5 + n_6$ is the total order of polynomials which was restricted to be less than or equal to eight. The distances are defined as follows: $r_1 = r_{\text{HH'}}$, $r_2 = r_{\text{HF}}$, $r_3 = r_{\text{HF'}}$, $r_4 = r_{\text{H'F}}$, $r_5 = r_{\text{HF'}}$, and $r_6 = r_{\text{FF'}}$. The multinomial basis functions in eqn. 1 are given in the symmetrized form,[23] and thus are invariant with respect to interchange of like atoms.

A total of 28,328 MRCI energies were sampled to determine the expansion coefficients of the polynomial. First, roughly 7000 and 8300 points were sampled in the vicinity of the transition state and the minimum energy path (MEP), respectively. These points were generated by random Cartesian displacements (of 0–0.3 Å) to the saddle point geometry and the geometries along the MEP, with a constraint that the HH, HF, and FF bond lengths cannot be shorter than 0.5, 0.5, and 1.0 Å, respectively. An additional ~1700 points were sampled on a three-dimensional grid created by the HH, HF, and FF bond lengths in the collinear H-H-F-F

configuration with a grid spacing of 0.1 Å.

The points in the reactants region were augmented by ~6000 points sampled using the diatom–diatom (HH–FF) Jacobi coordinate. The ranges of the variables were $0.5 \le r_{HH}/Å \le 3.0$, $1.0 \le r_{FF}/Å \le 4.0$, $0.0 \le R_{HH–FF}/Å \le 8.0$, $-\pi/2 \le \theta_1 \le \pi/2$, $-\pi/2 \le \theta_2 \le \pi/2$, and $0 \le \phi_1 \le \pi$, where $R_{HH–FF}$ is the distance between the centers of masses of HH and FF, θ_1 and θ_2 are the angles made by $R_{HH–FF}$ with r_{HH} and r_{FF}, respectively, and ϕ_1 is the torsional angle that r_{HH} makes with r_{FF}. The products region was described by the internal coordinate defined by the HH, HF, and FF bond lengths, HHF (a_{HHF}) and HFF (a_{HFF}) bond angles, and torsional angle ϕ_1. Approximately 3800 points were sampled using this coordinate with the variable ranges of $0.4 \le r_{HH}/Å \le 6.0$, $0.4 \le r_{HF}/Å \le 2.0$, $1.0 \le r_{FF}/Å \le 6.0$, $\pi/2 \le a_{HFF} \le \pi$, $\pi/2 \le a_{HHF} \le \pi$, and $0 \le \phi \le \pi$. For the sake of completeness, ~1400 points sampled in the HF dimer region were also added, which were generated using the HF–HF Jacobi coordinate with $0.4 \le r_{HF}/Å \le 2.4$, $1.0 \le R_{HF\text{-}HF}/Å \le 8.0$, $-\pi/2 \le \theta_3 \le \pi/2$, $-\pi/2 \le \theta_4 \le \pi/2$, and $0 \le \phi_2 \le \pi$, where $R_{HF–HF}$ is the distance between the centers of masses of two HF and the angles are defined in the same way as the HH–FF Jacobi coordinate.

The energy distribution of the sampled MRCI energies, relative to the reactant bottom, is shown in Figure 2. Most of the sampled points have an energy in the range 0–300 kJ mol^{-1}. The large peak found at the energy of ~100 kJ mol^{-1} corresponds to the points generated in the vicinity of the transition state. The distribution below 0 kJ mol^{-1} originates from the energies in the HF dimer region. The expansion coefficients for the 883 permutationally invariant terms in eqn. 1 were determined by a weighted least squares fit to these MRCI energies. The weights were defined as $w = E_w / [E_w + (V - E_{w'})]$ if $V > E_{w'}$ otherwise $w = 1$, where $E_w = 120$ kJ mol^{-1}, $E_{w'} = 240$ kJ mol^{-1}, and V is the MRCI potential energy relative to $H_2 + F_2$. The least squares

problem was solved by the singular value decomposition method using the LAPACK routines.[24]

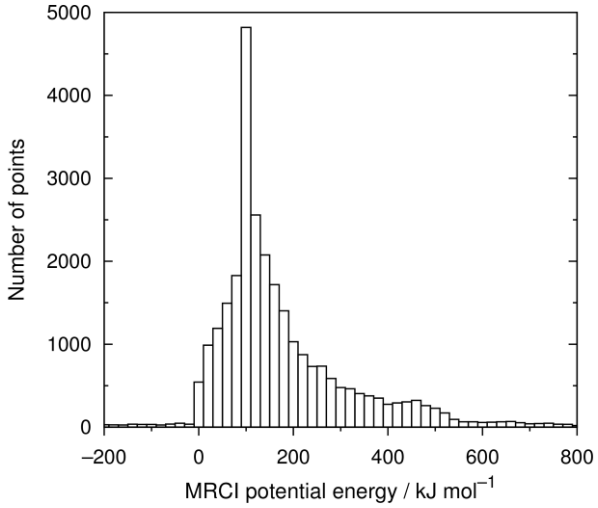

Figure 2. Distribution of MRCI energies used in the fit. The energies are relative to the bottom of the $H_2 + F_2$ reactants.

2.3. Quasiclassical Trajectory

QCT calculations were performed on the fitted PES. The reactions with various vibrational states of H_2 and F_2, (v_{HH}, v_{FF}), were investigated. The initial conditions were generated using a Monte Carlo sampling method.[25] The rotational quantum numbers of H_2 and F_2 were sampled from the Boltzmann distribution specified by temperatures T of 700, 1000, 1400, and 2000 K. The vibrational phases and rotational orientation of the initial reactants were selected at random. The relative translational energies between the reactants, E_{rel}, were sampled using the probability density function of $p(E_{rel}) = E_{rel} / (k_B T)^2 \exp(-E_{rel} / k_B T)$ with constraint of the form $E_{rel} \geq V^{\ddagger} - E_{vib}$, where k_B is the Boltzmann constant, $V^{\ddagger}$ is the potential barrier height and E_{vib} is the total vibrational energy of the H_2 and F_2 reactants.

The trajectories were initiated at a center of mass distance between the reactants of 7.9 Å,

propagated using the fourth-order symplectic integrator[26] with a time step of 0.1 fs, and terminated when products reached a separation of 13.2 Å. The energy gradients were calculated analytically from eqn. 1. To improve the convergence, the impact parameter b was uniformly sampled over 0–b_{max}, rather than sampling b^2 uniformly over 0–b_{max}^2.[27] The maximum impact parameter b_{max} was set to 2.1, 3.2, and 4.2 Å for the trajectories with $v_{FF} \leq 2$, $3 \leq v_{FF} \leq 8$, and $v_{FF} \geq 9$, respectively.

The reaction probability for each ensemble (specified by T, v_{HH}, and v_{FF}) was calculated as

$$P_r = P_{base} \frac{1}{N_{total}} \sum_{i}^{N_r} w_i \tag{2}$$

where N_{total} is the total number of trajectories of each ensemble, N_r is the number of reactive trajectories, w_i are the statistical weights for the ith reactive trajectories, $w_i = 2b_i / b_{max}$ (to correct the biased selection of the impact parameter[27]), and P_{base} is the factor that corrects the constraint sampling of E_{rel},

$$P_{base} = \begin{cases} 1 & (\text{if } V^{\ddagger} < E_{vib}) \\ \displaystyle\int_{V^{\ddagger} - E_{vib}}^{\infty} p(E_{rel})\, \mathrm{d}E_{rel} & (\text{otherwise}) \end{cases} \tag{3}$$

The corresponding rate constants can be obtained by,

$$k(T) = \left(\frac{8k_B T}{\pi \mu_R}\right)^{1/2} \pi b_{max} P_r \tag{4}$$

where μ_R is the reduced mass of the reactants. Batches of 10^5–10^7 trajectories were calculated

for each ensemble.

The collinear reaction probabilities were also calculated by QCT to compare the results with the QM calculation. In this calculation, the trajectories were restricted to propagate on the collinear H-H-F-F configuration. The initial conditions were generated by explicitly specifying E_{rel}, v_{HH}, and v_{FF}. Only the vibrational phases of the reactants were selected at random. The integration method was the same as the full-dimensional calculation. An ensemble of 10^4 trajectories was calculated for each combination of E_{rel}, v_{HH}, and v_{FF}. The collinear reaction probabilities at the relative translational energies E_{rel} and at temperature T were given as:

$$P_{\text{collinear}}(E_{\text{rel}}) = \frac{N_{\text{r}}(E_{\text{rel}})}{N_{\text{total}}} \tag{5}$$

$$P_{\text{collinear}}(T) = \frac{1}{k_{\text{B}}T}\int_0^{\infty} P_{\text{collinear}}(E_{\text{rel}})\exp(-E_{rel}/k_{\text{B}}T)\ \mathrm{d}E_{\text{rel}} \tag{6}$$

Error limits reported with the QCT results are one standard deviation throughout the paper.

2.4. Quantum Mechanical Reactive Scattering

A reduced dimensionality QM reactive scattering calculation was carried out for R1. The system was treated as a collinear four-atom reaction of type AB + CD → A + BCD, where the HF + F fragments were represented as HFF. The Hamiltonian for the reactant and product arrangements of this system can be written in the mass-scaled Jacobi coordinates described in ref. 28. To solve the Schrödinger equation, the Hamiltonian expressed in the hypercylindrical coordinate system,[28] (ρ, θ, z), was employed, where ρ is the hyperradius, θ is the hyperangular

variable that connects the two arrangements, and z is the mass-scaled internuclear distance of FF. The continuum states that arise from the dissociation of FF were approximated by discrete eigenstates using a finite-size grid along the z coordinate ranging from z_{min} = 3.2 a.u. to z_{max} = 21.3 a.u. (corresponding to r_{FF} = 0.8–5.3 Å).

The R-matrix propagation method[29] was used to solve the close-coupling equations. The two-dimensional eigenvalue problems at fixed ρ were solved by the discrete variable representation method[30] using the particle-in-a-box basis with 400 and 200 functions for the θ and z coordinates, respectively. The R-matrix was propagated for 840 evenly-spaced sectors from ρ = 3.8 to 24.8 a.u.. The lowest 500 eigenstates were used for the propagation. The collinear reaction probabilities were obtained by applying the scattering boundary conditions, averaged for ρ = 23.5–24.8 a.u., and summed over the final states.

Convergence was ensured through comparison of the results obtained with different numbers of channels and basis functions. Also, the reaction probabilities were found to be insensitive to the value of z_{max}, indicating the validity of the approximation made for the three-body dissociation.

2.5. Transition State Theory

Thermal rate constants for R1 were also calculated by conventional TST. The partition functions for the reactants and transition state were evaluated using the rigid-rotor-harmonic-oscillator approximation, except for the bending modes of the transition state. The rotational constants and harmonic frequencies for H_2 and F_2 were taken from experimental values.[20] The reaction barrier height and the properties for the transition state were

calculated on the fitted PES. A one-dimensional semiclassical tunneling correction was made by assuming an asymmetric Eckart potential.[31] As suggested in previous studies on collinear hydrogen abstraction reactions from H_2,[32,33] anharmonic treatment of the bending vibrations of the transition state is important for reactions involving external hydrogen abstraction. Therefore, the partition functions for the bending vibrations were directly evaluated from the vibrational eigenstates calculated by solving the Schrödinger equation on the relaxed potential curves along the bending coordinates, using the BEx1D program.[34]

3. Results and Discussion

3.1. Accuracy and Properties of the Potential Energy Surface

The root-mean-squares fitting error of the PES for the points below 300 kJ mol^{-1} (relative to the reactants) is 2.74 kJ mol^{-1}. Figure 3(a) shows the potential energies on the fitted PES (V_{PES}) plotted as a function of the MRCI potential energies (V_{MRCI}). All of the points lie close to the ideal line with no significant outlier. Distribution of the deviations ($\Delta V = V_{PES} - V_{MRCI}$) for these points is shown in Figure 3(b). The maximum absolute deviation is 17.3 kJ mol^{-1}. More than 92 and 99% of the points have absolute deviations less than 5 and 10 kJ mol^{-1}, respectively. Therefore, the fitted PES is globally accurate and considered suitable for the dynamical studies.

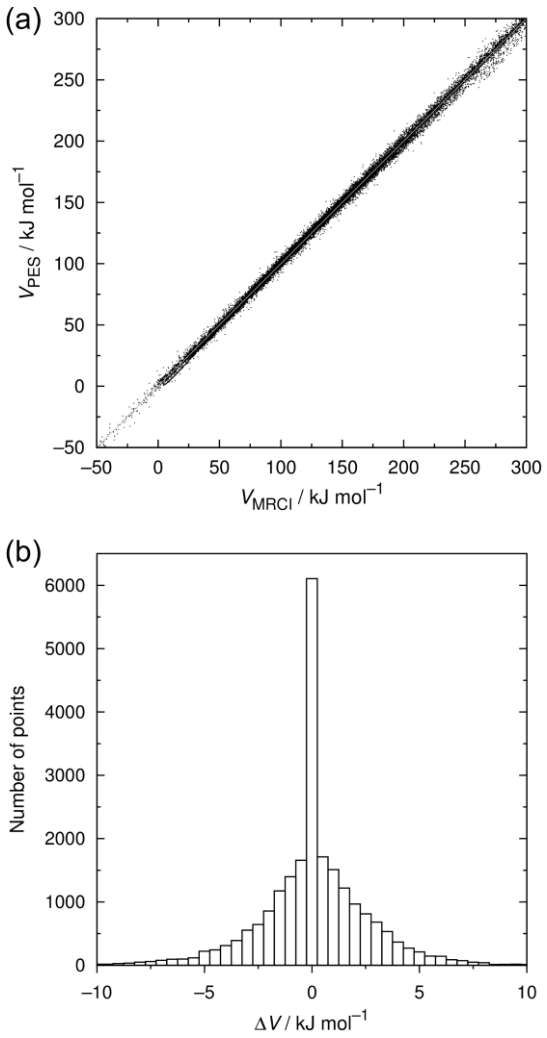

Figure 3. (a) Potential energies on the fitted PES as a function of those calculated at the MRCI level. (b) Distribution of the energy deviations.

The geometries and harmonic vibrational frequencies of the reactants, products, and transition state are shown in Tables 1 and 2. As seen, the fitted PES accurately reproduces the MRCI bond lengths for all of the structures within errors of 0.1%. The vibrational frequencies calculated on the PES are also in good agreement with the MRCI values with deviations of only a few tens of

cm^{-1}, except for the imaginary frequency of the transition state. Furthermore, both the PES and MRCI results for the diatomic molecules are in excellent agreement with the experimental bond lengths and frequencies[20] as shown in Table 1. Figure 4 shows the potential energy curves along the MEP calculated on the fitted PES and by the MRCI method. Although the PES underestimates the imaginary frequency corresponding to motion along the reaction coordinate by 150*i* cm^{-1}, there is good agreement between the two potential curves. The difference in the imaginary frequencies reflects the slightly widened peak at the saddle point observed on the fitted PES compared to the MRCI. The potential barrier height and reaction energy on the fitted PES are 115 and 30 kJ mol^{-1}, respectively, which reproduce well the MRCI results of 112 and 25 kJ mol^{-1}, respectively. Also, the non-existence of the trapezoidal transition state[1] was ascertained as described in the ESI (Figure S1).

Table 1. Equilibrium bond lengths (Å) and harmonic vibrational frequencies (cm^{-1}) of H_2, F_2, and HF.

	PES[a]	MRCI[b]	exp.[c]
$r(H_2)$	0.7415	0.7416	0.74144
$r(F_2)$	1.4090	1.4101	1.41193
r(HF)	0.9157	0.9163	0.91681
$\omega(H_2)$	4384	4402	4401.2
$\omega(F_2)$	924	918	916.6
ω(HF)	4113	4153	4138.3

[a] Properties on the fitted PES.

[b] MRCI-F12(CV)+Q/cc-pCVTZ-F12.

[c] Experimental values taken from ref. 20.

Table 2. Structure (bond lengths in Å) and harmonic vibrational frequencies (cm^{-1}) of the

transition state for R1.

	PES[a]	MRCI[b]
r_{HH}	0.8654	0.8654
r_{FF}	1.7290	1.7292
r_{HF}	1.1603	1.1591
ω_1 rc[c]	1465*i*	1615*i*
ω_2 HH str.	2045	2025
ω_3 FF str.	656	658
ω_4 bend.	313	268
ω_5 bend.	301	300

[a] Properties on the fitted PES.

[b] MRCI-F12(CV)+Q/cc-pCVTZ-F12.

[c] Reaction coordinate.

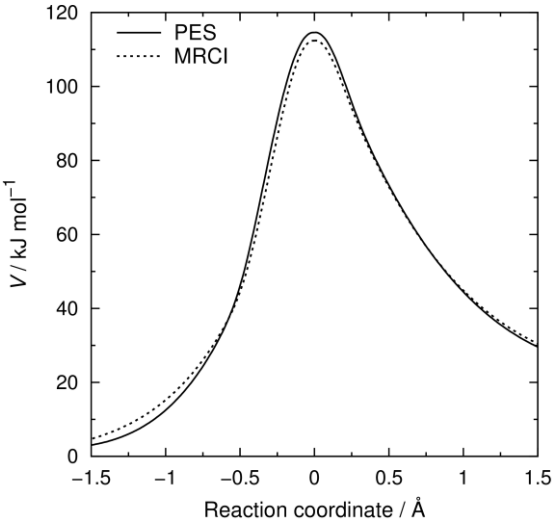

Figure 4. Potential energy curves along the MEP calculated on the fitted PES and by the MRCI method. The energies are relative to the reactants.

Figure 5 shows the potential energies calculated along the two degenerate bending coordinates of the transition state. Normal-mode analyses at the transition state indicated that the normal coordinates for the bending vibrations can be approximated by the internal coordinates, α and β, shown in Figure 5; therefore, the energy curves were calculated as a function of either of the angles α or β, with the other structural parameters relaxed by saddle-point optimizations. The α- and β-bending modes correspond to the harmonic vibrational frequencies ω_4 and ω_5, respectively, shown in Table 2. The energies on the fitted PES fall approximately in line with the MRCI points. The lines shown in Figure 5 are fits of the PES energies to potential functions in the power series of either $\cos\alpha$ or $\cos\beta$. The vibrational eigenstates for these potential functions were calculated by expanding the wave functions with the associated Legendre basis functions. For the β-bending mode, the vibrational eigenstates are similar to those calculated using the harmonic oscillator approximation, and the difference between the anharmonic and harmonic vibrational partition functions is, at most, only 5% over the temperature range 300–2000 K. Conversely, the energy curve of the α-bending mode is highly anharmonic, with ratios of the anharmonic to harmonic partition function of 0.72, 0.47, and 0.33 at 300, 1000, and 2000 K, respectively.

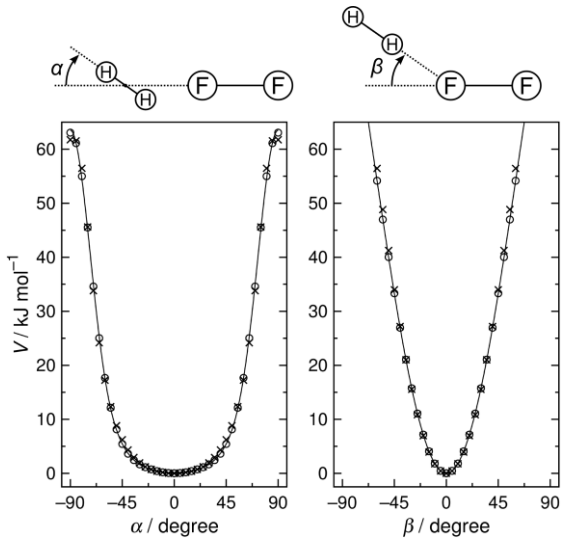

Figure 5. Potential energy curves along the approximate bending coordinates of the transition state calculated on the fitted PES (circles) and by the MRCI method (crosses). The lines represent the fits to the potential functions (see main text).

Shown in Figure 6 are the equipotential contour plots in which the energies are shown as functions of r_{HH} and r_{HF} (a), and r_{FF} and r_{HF} (b). In these contours, the four atoms were kept collinear and the other internal coordinates were relaxed; specifically, r_{FF} and r_{HH} were optimized in (a) and (b), respectively. Again, there is good agreement between the fitted PES and the MRCI energies. As expected from the reaction energetics, the saddle point is located at the middle of the reaction coordinate. The ratio of the bond lengths at the transition state (Table 2) to those of the fragments (Table 1) are 1.17, 1.23, and 1.27 for HH, FF, and HF, respectively, indicating that the reaction has a "central" barrier where both the HH and FF bonds are simultaneously elongated while the HF bond is shortened. Therefore, in the context of the Polanyi rule[35] proposed for triatomic reactions, the vibrational excitation of either or both of the reactants is expected to have a moderate effect on the reactivity, possibly comparable to that

attained by increasing the translational energy.

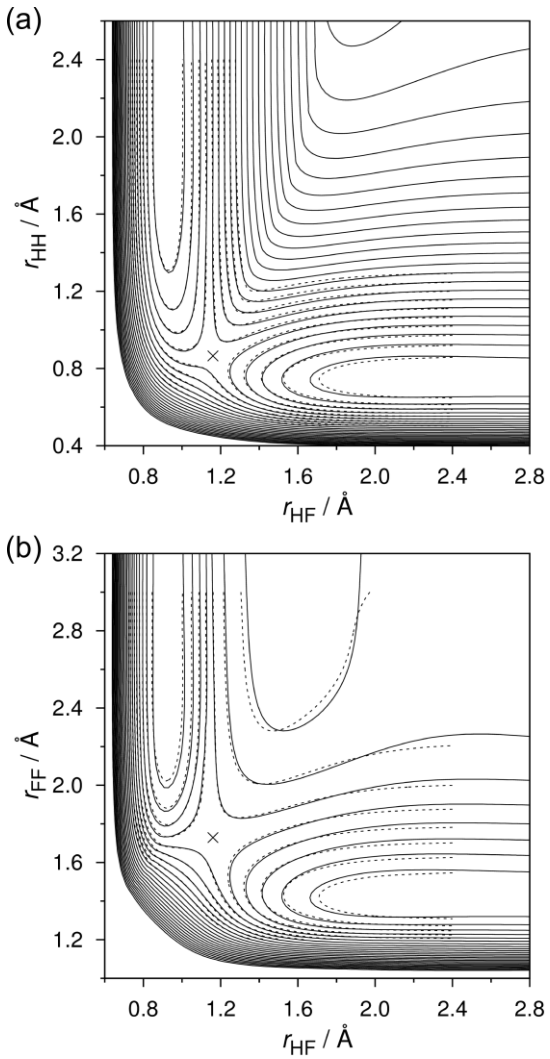

Figure 6. Equipotential contour plots of the $H_2 + F_2 \rightarrow H + HF + F$ reaction on the collinear configuration with the coordinate r_{FF} and r_{HH} optimized in (a) and (b), respectively. The solid and dotted contours are the results for the fitted PES and the MRCI calculation, respectively. The cross symbols represent the saddle point. The contour increments are 20 kJ mol^{-1}.

3.2. Collinear Reaction Probability

The reaction probabilities on the collinear configuration were calculated by the QM reactive scattering and QCT methods for the reactant vibrational states, (v_{HH}, v_{FF}), of (0, 0–9) and (1, 0–3). The results are plotted in Figure 7 as a function of the total (sum of the initial vibrational and relative translational) energy up to 220 kJ mol^{-1}. The dependencies on the translational energy are also plotted in Figure S2 in the ESI. The QM calculations predict reaction thresholds of ~120 and ~150 kJ mol^{-1} for the reactions with v_{HH} = 0 and 1, respectively. Though they are higher than the classical barrier (115 kJ mol^{-1}), the threshold for v_{HH} = 0 is significantly lower than the zero-point energy (ZPE)-corrected energy of the transition state relative to the potential bottom of the reactants (131 kJ mol^{-1}, excluding ZPEs for the bending modes), indicating a substantial tunneling effect. Interestingly, the QCT results with the high vibrational excitation of F_2 are in good agreement, albeit slightly overestimating, with the reaction thresholds predicted by QM. This may be due to a fortunate error cancellation resulting from the lack of quantum effects and the violation of ZPE in the vicinity of the transition state. As a whole, the QCT results are comparable to the QM reaction probabilities, though the reaction thresholds and the peak reaction probabilities for the states (v_{HH}, v_{FF}) = (0, 2) and (1, 1) are overestimated. Also, in the QCT calculation, there was no reactive trajectory found for the states (0, 0), (0, 1), and (1, 0); their reaction probabilities are estimated to be less than 10^{-4}. In contrast, the QM results show small but discernable reaction probabilities for these states; for example, the QM reaction probabilities at the total energy of 200 kJ mol^{-1} are ~0.001, ~0.01, and ~0.02 for (0, 0), (0, 1), and (1, 0), respectively. This discrepancy signifies the limitation of the classical treatment for the states with low reaction probabilities.

Both the QM and QCT calculations demonstrate that the vibrational excitations of F_2 dramatically promote the reaction. Vibrational excitation of H_2 raise the reaction threshold in terms of the total energy, but lower the threshold in terms of the relative translational energy, considering the energy gap of H_2 between $v_{HH} = 0$ and 1 (see Figure S2 in the ESI). Nonetheless, enhancement of the reactivity by H_2 vibrational excitation is limited compared to F_2 excitation, and is not expected to be as efficient as increasing the translational energy by an equivalent amount. It should be noted that the difference in reaction thresholds (in terms of the total energy) between $v_{HH} = 0$ and 1 is ~30 kJ mol^{-1}, which is comparable to the difference in the vibrationally adiabatic barrier heights of 25 kJ mol^{-1} estimated based on the harmonic frequency for the H–H stretching mode of the transition state.

Figure 8 shows the collinear reaction probabilities thermally averaged over the relative translational energies (using eqn. 6) at 1000 and 2000 K, as a function of the initial vibrational energy of the reactants. QCT results show excellent agreement with the QM results, except for the states (0, 0), (0, 1), and (1, 0), for which no reactive trajectory was found. Again, the vibrational excitations of both H_2 and F_2 enhance the reactivity, and the effect is considerably larger in the F_2 excitation than for H_2. For example, at 1000 K, the reaction probability for the (0, 5) state is approximately three orders of magnitude larger than that for (1, 0) which has the vibrational energy comparable to the (0, 5) states. The agreement between the QM and QCT collinear reaction probabilities supports the applicability of the QCT method for investigating the full-dimensional reaction dynamics and kinetics of R1.

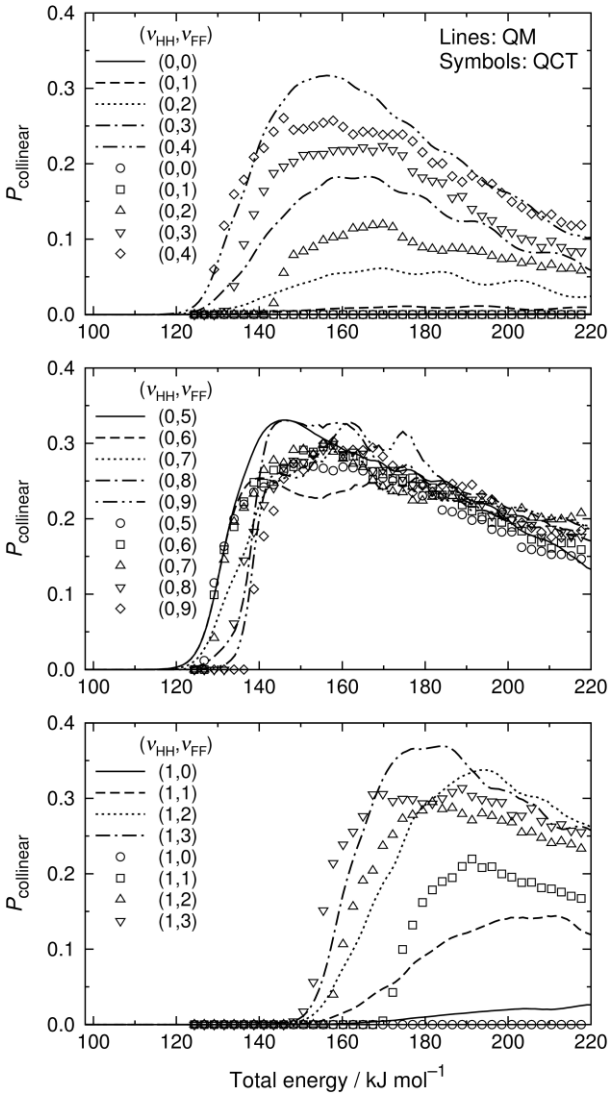

Figure 7. Collinear reaction probabilities for R1 as a function of the total energy relative to the reactants.

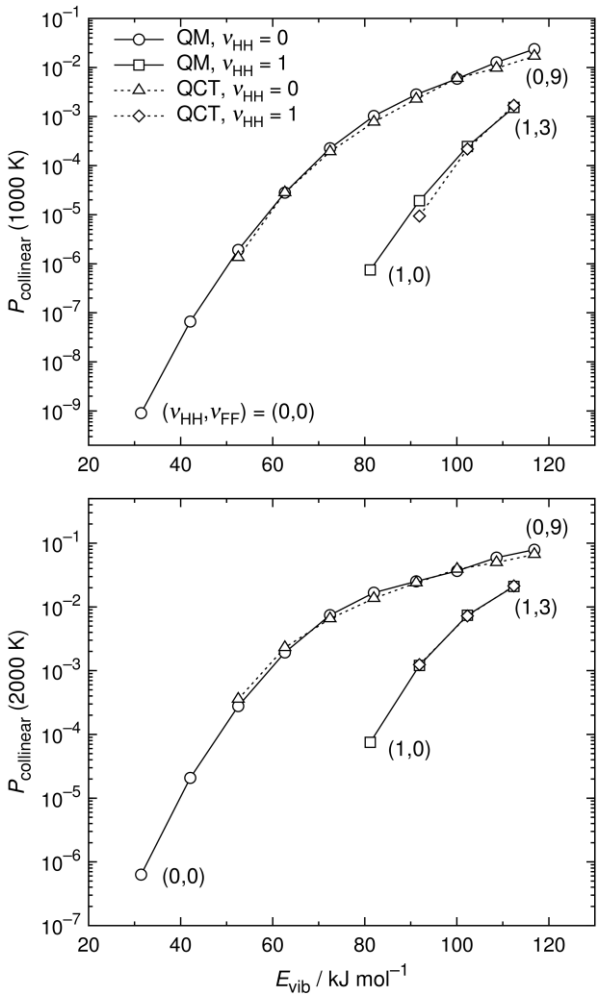

Figure 8. Collinear reaction probabilities for R1 thermally averaged over the relative translational energies as a function of the reactants vibrational energy at 1000 (top) and 2000 K (bottom).

3.3. Full-Dimensional QCT and Rate Constants

The state-specific rate constants for R1 at the temperatures of 1000 and 2000 K obtained from the full-dimensional QCT calculations are shown in Figure 9 as a function of the initial vibrational energy of the reactants. The calculations were performed for the reactants' vibrational states of v_{HH} = 0–2 and v_{FF} = 0–12. At 1000 K, the rate constants for the states (v_{HH},

v_{FF}) = (0, 0) and (1, 0) are not plotted because of the absence of the reactive trajectory within $N_{total} = 10^7$; their upper limits are estimated to be 2×10^{-20} and 4×10^{-18} cm^3 molecule^{-1} s^{-1}, respectively. Conversely, at 2000 K, there were 19 and 59 reactive trajectories from the ensembles of 10^6 trajectories for the states (0, 0) and (1, 0), respectively, and converged rate constants were obtained for these states. The dependence of the rate constants on the initial vibrational energy is consistent with that observed for the collinear reaction probabilities (Figure 8).

Previous kinetic modeling studies[1,2] suggested the reaction of vibrationally excited H_2 with thermal F_2 as being a critical chain-branching step in the H_2/F_2 reaction system. To examine the proposed kinetic model, state-specific QCT rate constants calculated at temperatures of 700, 1000, 1400, and 2000 K were thermally averaged over v_{FF} using the Boltzmann weights, and are plotted in Figure 10. Though the QCT rate constants could not be obtained for the low vibrational states of the reactants at temperatures of 700 and 1000 K, their contributions to the rate constants shown in Figure 10 were estimated from their upper limits and found to be negligible. As expected, the rate constants monotonically increased by increasing v_{HH} from 0 to 2. However, the predicted rate constants for $H_2(v_{HH} = 1) + F_2$ are significantly smaller than that used in the previous kinetic modeling study.[1] It was found from the calculated QCT rate constants that a single increment of v_{HH} results in a factor of approximately exp(2200/T) increase in the rate constants, which corresponds to lowering the barrier height by 18 kJ mol^{-1}. This value is considerably smaller than the energy gap of 50 kJ mol^{-1} between $H_2(v_{HH} = 1)$ and the ground-state H_2; therefore, the vibrational excitation of H_2 is not as efficient as the translational energy in promoting the reaction.

The cross symbols in Figure 10 represent the fully thermal QCT rate constants (thermally

averaged over both v_{HH} and v_{FF}). The thermal QCT rate constants are slightly smaller than the TST rate constants, particularly at 700 K, possibly because of the quantum tunneling effect. Nevertheless, the rate constants agree within a factor of two, corroborating the accuracy of the QCT rate constants.

It should be noted here that there are other product channels accessible in the collision of H_2 with F_2. Figure 11 shows the rate constants for the three product channels observed in the full-dimensional QCT calculation at the temperature of 1000 K and $v_{HH} = 1$. The H + HF + F channel (R1) is dominant in most cases; however, the branching fraction for the H_2 + F + F channel becomes increasingly larger at high v_{FF}, and dominates over the H + HF + F channel at $v_{FF} > 10$. This H_2 + F + F channel represents a collision-induced dissociation of F_2 by H_2, and is expected to be easily accessible at high v_{FF} due to the small bond dissociation energy of F_2. Though the contribution is small, there are some trajectories leading to the HF + HF products. Inspection of these trajectories revealed that the formation of two HF is due to the association of H and F atoms beyond the transition state of R1; namely, the first HF is formed as in the case of R1, followed by the second HF formation in the post-transition-state region. This channel represents another example of the post-transition-state dynamics,[36] but is expected to play only a minor role in this reaction due to the small branching fractions.

To summarize the results, the rate constants for R1 can be enhanced by the vibrational excitation of H_2 and F_2, but the effect is limited in the H_2 excitation compared to F_2. The QCT calculation suggests that the rate constants for R1' used in the previous kinetic modeling study[1] were likely to be overestimated. However, the vibrational excitation of F_2, rather than H_2, was found to dramatically promote the H_2 + F_2 reaction; therefore, this study proposes the reactions of vibrationally non-equilibrium F_2 with H_2, which was not considered in the previous study,[1] as

an alternative chain-branching reaction in the combustion of H_2/F_2 mixtures.

A straightforward application of the Polanyi rule[35] would suggest that the vibrational excitation of either H_2 or F_2 is expected to have an effect comparable to the translational energy in promoting the reaction. This study clearly demonstrates that excitation of H_2 vibration is considerably less efficient than the translational energy, whereas excitation of F_2 vibration is significantly effective. The preference for the F_2 excitation can be qualitatively explained from the geometry of the transition state where the HH and FF bond lengths are elongated by 17 and 23%, respectively, from the reactants. However, such a large difference in the reactivity is not expected. The mode selective reactivity of bimolecular reactions should not be interpreted only from the location of the reaction barrier, but also in terms of the coupling between vibrational modes and the reaction coordinate.[37,38] The present results indicate that the F_2 vibration is strongly coupled with the reaction coordinate, but the coupling between the H_2 vibration and the reaction coordinate motion is modest. A simple yet persuasive explanation, which can also be inferred from the potential contour plots shown in Figure 6, is that 67 kJ mol^{-1} of energy is needed to elongate the bond length of an isolated F_2 molecule by 23% from its equilibrium, whereas only 21 kJ mol^{-1} is needed to elongate H_2 by 17%. This observation illustrates the importance of insights from the PES topography to elucidate the mode coupling in the vicinity of the transition state, and will deepen our understanding of the mode-selectivity in bimolecular reactions.

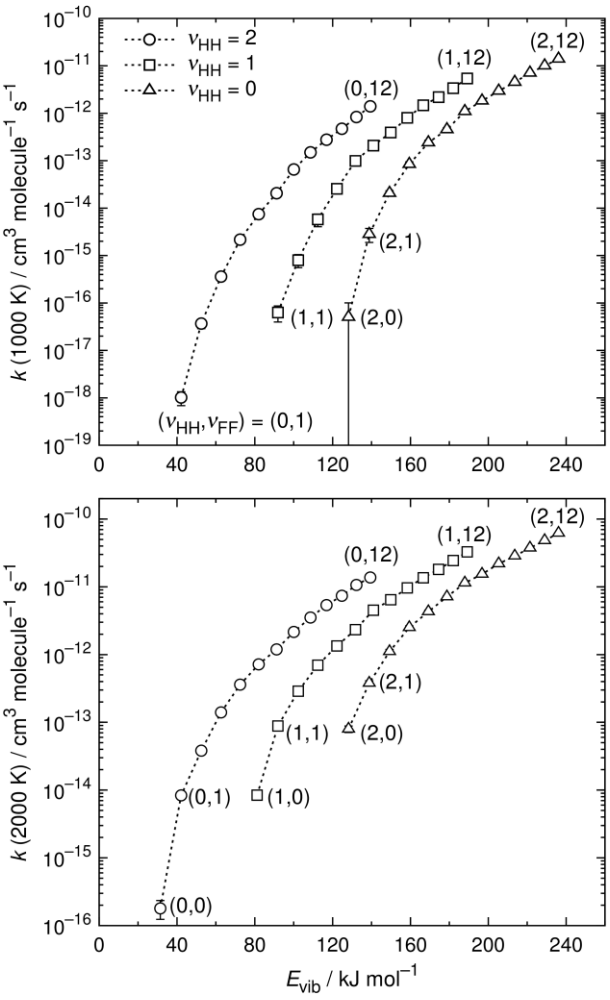

Figure 9. State-specific QCT rate constants for R1 as a function of the reactant vibrational energy at 1000 (top) and 2000 K (bottom).

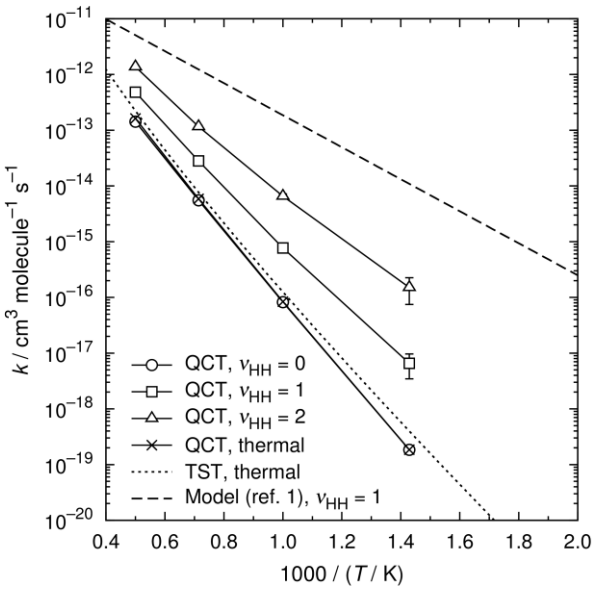

Figure 10. Arrhenius plot of the QCT and TST rate constants for R1. Open symbols represent the rate constants thermally averaged over v_{FF}. Cross symbols and the dotted line are the thermal rate constants calculated by QCT and TST, respectively. Dashed line is the rate constant for R1' used in the previous kinetic modeling study.[1]

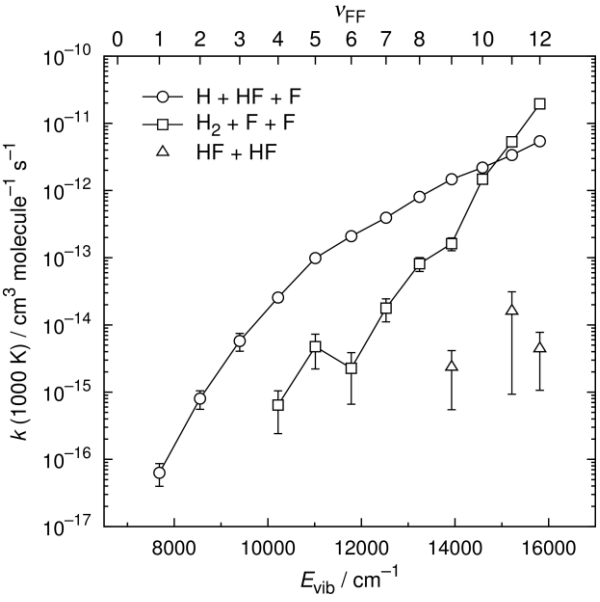

Figure 11. QCT rate constants for the three product channels in the reaction between H_2 and F_2 as a function of reactant vibrational energy at 1000 K and $v_{HH} = 1$.

4. Conclusion

A global potential energy surface describing the reaction $H_2 + F_2 \rightarrow H + HF + F$ (R1) was constructed on the basis of quantum chemical calculation at the MRCI-F12(CV)+Q / cc-pCVTZ-F12 level. A total of 28,328 MRCI energies were fitted to a polynomial represented by direct products of Morse variables for the six internuclear distances. The PES was used to investigate the dynamics of R1 by the QCT and QM scattering methods. The collinear reaction probabilities were calculated by QCT and QM calculations, and the vibrational state specific rate constants were evaluated by full-dimensional QCT calculations. Both the collinear and full-dimensional results demonstrate that R1 can be significantly promoted by the vibrational excitation of F_2. Though excitation of the H_2 vibration was also found to enhance the reactivity, the effect is limited and not as efficient as increasing the translational energy by an equivalent amount. These results indicate that the rate constants for the presumed chain-branching reaction in the H_2/F_2 combustion, H_2 ($v = 1$) + $F_2 \rightarrow H + HF + F$ (R1'), used in the previous kinetic modeling study[1] were overestimated, and the alternative chain-branching mechanism, the reactions of vibrationally non-equilibrium F_2 with H_2, is proposed. The mode-selective reactivity observed for R1 was explained in terms of the coupling between the vibrational modes of the reactants and the reaction coordinate motion.

Acknowledgement

The authors thank Dr. Akira Miyoshi (University of Tokyo) for helpful discussions.

References

1 A. Matsugi, H. Shiina, K. Tsuchiya and A. Miyoshi, *J. Phys. Chem. A*, 2013, **117**, 14042–14047.

2 J. H. Sullivan, R. C. Feber and J. W. Starner, *J. Chem. Phys.*, 1975, **62**, 1714–1725.

3 J. F. Bott and N. Cohen, *J. Chem. Phys.*, 1973, **58**, 4539–4549.

4 N. Cohen and J. F. Bott, *Review of Rate Data for Reactions of Interest in HF and DF Lasers*, Report No. SD-TR-82-86; Aerospace Corp., El Segundo, CA, 1982.

5 G. A. Kapralova, E. M. Margolina and A. M. Chaikin, *Kinet. Catal.*, 1969, **10**, 23–27.

6 V. L. Orkin and A. M. Chaikin, *Kinet. Catal.*, 1979, **20**, 1129–1135.

7 D. L. Thompson and D. R. McLaughlin, *J. Chem. Phys.*, 1975, **62**, 4284–4299.

8 H.-J. Werner and P. J. Knowles, *J. Chem. Phys.*, 1988, **89**, 5803–5814.

9 P. J. Knowles and H.-J. Werner, *Chem. Phys. Lett.*, 1988, **145**, 514–522.

10 T. Shiozaki, G. Knizia and H.-J. Werner, *J. Chem. Phys.*, 2011, **134**, 034113.

11 J. Almlöf, B. J. Deleeuw, P. R. Taylor, C. W. Bauschlicher Jr and P. Siegbahn, *Int. J. Quantum Chem.*, 1989, **36**, 345–354.

12 K. A. Peterson, R. A. Kendall and T. H. Dunning Jr, *J. Chem. Phys.*, 1993, **99**, 9790–9805.

13 L. Kong, F. A. Bischoff and E. F. Valeev, *Chem. Rev.*, 2011, **112**, 75–107.

14 T. Shiozaki and H.-J. Werner, *Mol. Phys.*, 2013, **111**, 607–630.

15 J. G. Hill, S. Mazumder and K. A. Peterson, *J. Chem. Phys.*, 2010, **132**, 054108.

16 F. Weigend, *Phys. Chem. Chem. Phys.*, 2002, **4**, 4285–4291.

17 F. Weigend, A. Kohn and C. Hattig, *J. Chem. Phys.*, 2002, **116**, 3175–3183.

18 C. Hattig, *Phys. Chem. Chem. Phys.*, 2005, **7**, 59–66.

19 H.-J. Werner, P. J. Knowles, G. Knizia, F. R. Manby, M. Schütz, P. Celani, T. Korona, R. Lindh, A. Mitrushenkov, G. Rauhut, K. R. Shamasundar, T. B. Adler, R. D. Amos, A. Bernhardsson, A. Berning, D. L. Cooper, M. J. O. Deegan, A. J. Dobbyn, F. Eckert, E. Goll, C. Hampel, A. Hesselmann, G. Hetzer, T. Hrenar, G. Jansen, C. Köppl, Y. Liu, A. W. Lloyd, R. A. Mata, A. J. May, S. J. McNicholas, W. Meyer, M. E. Mura, A. Nicklaß, D. P. O'Neill, P. Palmieri, D. Peng, K. Pflüger, R. Pitzer, M. Reiher, T. Shiozaki, H. Stoll, A. J. Stone, R. Tarroni, T. Thorsteinsson and M. Wang, MOLPRO, version 2012.1, Cardiff, 2012.

20 K. P. Huber and G. Herzberg, *Molecular Spectra and Molecular Structure, IV. Constants of Diatomic Molecules*, Van Nostrand Reinhold, New York, 1979.

21 S. Zou and J. M. Bowman, *Chem. Phys. Lett.*, 2003, **368**, 421–424.

22 X. Zhang, S. Zou, L. B. Harding and J. M. Bowman, *J. Phys. Chem. A*, 2004, **108**, 8980–8986.

23 B. J. Braams and J. M. Bowman, *Int. Rev. Phys. Chem.*, 2009, **28**, 577–606.

24 E. Anderson, Z. Bai, C. Bischof, S. Blackford, J. Demmel, J. Dongarra, J. Du Croz, A. Greenbaum, S. Hammarling, A. McKenney and D. Sorensen, *LAPACK Users' Guide, 3rd ed.*, Society for Industrial and Applied Mathematics, Philadelphia, 1999.

25 G. H. Peslherbe, H. Wang and W. L. Hase, *Adv. Chem. Phys.*, 2007, **105**, 171–201.

26 H. Yoshida, *Phys. Let. A*, 1990, **150**, 262–268.

27 M. B. Faist, J. T. Muckerman and F. E. Schubert, *J. Chem. Phys.*, 1978, **69**, 4087–4096.

28 Q. Sun and J. M. Bowman, *J. Chem. Phys.*, 1990, **92**, 1021–1029.

29 J. C. Light and R. B. Walker, *J. Chem. Phys.*, 1976, **65**, 4272–4282.

30 J. C. Light, I. P. Hamilton and J. V. Lill, *J. Chem. Phys.*, 1985, **82**, 1400–1409.

31 B. C. Garrett and D. G. Truhlar, *J. Phys. Chem.*, 1979, **83**, 2921–2926.

32 M. Nakajima, A. Matsugi and A. Miyoshi, *J. Phys. Chem. A*, 2009, **113**, 8963–8970.

33 A. Matsugi, K. Suma and A. Miyoshi, *Phys. Chem. Chem. Phys.*, 2011, **13**, 4022–4031.

34 A. Miyoshi, BEx1D software, rev. 2008.10.08, available from the author. See http://www.frad.t.u-tokyo.ac.jp/~miyoshi/bex1d/.

35 J. C. Polanyi, *Acc. Chem. Res.*, 1972, **5**, 161–168.

36 U. Lourderaj, K. Park and W. L. Hase, *Int. Rev. Phys. Chem.*, 2008, **27**, 361–403.

37 S. Yan, Y.-T. Wu and K. Liu, *Proc. Nat. Acad. Sci.*, 2008, **105**, 12667–12672.

38 R. Liu, M. Yang, G. Czakó, J. M. Bowman, J. Li and H. Guo, *J. Phys. Chem. Lett.*, 2012, **3**, 3776–3780.